Materials Today Chemistry 9 (2018) 80–90

Contents lists available at ScienceDirect

Materials Today Chemistry

journal homepage: www.journals.elsevier.com/materials-today-chemistry/

A spontaneous solid-state NO donor to fight antibiotic resistant bacteria

Giuseppe Pezzotti [a, b, c, d]

[a] Ceramic Physics Laboratory, Kyoto Institute of Technology, Sakyo-ku, Matsugasaki, 606-8585 Kyoto, Japan
[b] Department of Orthopedic Surgery, Tokyo Medical University, 6-7-1 Nishi-Shinjuku, Shinjuku-ku, 160-0023 Tokyo, Japan
[c] The Center for Advanced Medical Engineering and Informatics, Osaka University, Yamadaoka, Suita, 565-0871 Osaka, Japan
[d] Department of Immunology, Graduate School of Medical Science, Kyoto Prefectural University of Medicine Kamigyo-ku, 465 Kajii-cho, Kawaramachi dori 602-0841 Kyoto, Japan

ARTICLE INFO

Article history:
Received 5 March 2018
Received in revised form
29 May 2018
Accepted 29 May 2018

Keywords:
Silicon nitride
Staphylococcus epidermidis
Antibacterial behavior
Raman spectroscopy

ABSTRACT

This study substantiates the chemical origin of a free-radical-driven antibacterial effect at the surface of biomedical silicon nitride (Si_3N_4) in comparison with the long-known effect of oxygen reduction by oxidized TiO_2 at the surface of biomedical titanium alloys. Similar to the antibacterial effect exerted by reactive oxygen species (ROS; i.e., superoxide anions, hydroxyl radicals, singlet oxygen, and hydrogen peroxide) from TiO_2, reactive nitrogen species (RNS), such as nitrous oxide (N_2O), nitric oxide (NO), and peroxynitrite ($^{-}$OONO) in Si_3N_4, severely affect bacterial metabolism and lead to their lysis. However, *in vitro* experiment with gram-positive *Staphylococcus epidermidis* (*S. epidermidis*, henceforth) revealed that ROS and RNS promoted different mechanisms of lysis. Fluorescence microscopy of NO radicals and *in situ* time-lapse Raman spectroscopy revealed different metabolic responses of living bacteria in contact with different substrates. After 48 h, the DNA of bacteria showed complete destruction on Si_3N_4, while carbohydrates of the peptidoglycan membrane induced bacterial degradation on Ti-alloy substrates. Different spectroscopic fingerprints for bacterial lysis documented the distinct effects of RNS and ROS. Spontaneously activated in aqueous environment, the RNS chemistry of Si_3N_4 proved much more effective in counteracting bacterial proliferation as compared to ROS formed on TiO_2, which requires external energy (photocatalytic activation) to enhance effectiveness. Independent of surface topography, the antibacterial effect observed on Si_3N_4 substrates is due to its unique kinetics ultimately producing NO and represents a new intriguing avenue to fight bacterial resistance to conventional antibiotics.

1. Introduction

Antimicrobial effects in synthetic biomaterials have been obtained through incorporation of specific chemical species at the surface finishing stage, or through exploiting the formation of reactive byproducts from surfaces exposed to biological environment [1]. Elution of antimicrobial agents from the biomaterial surface has mainly been pursued by incorporating covalently linked antibiotics [2–5]. However, the clinical effectiveness of this latter approach is limited by the sensitivity of bacteria to specific antibiotics and ultimately prone to antibiotic resistant mutations of bacterial strains. This requires the use of combinations of antibiotics in the clinical practice. Moreover, covalent binding is insufficiently sensitive to external stimuli [6], which requires designing adjuvant mechanisms of controlled drug release [7]. A popular contact-killing approach for biomaterial surfaces employs ROS as active substances. ROS arise from redox reactions between adsorbed species (such as water and oxygen) and electrons/holes at a solid surface. This approach has so far featured TiO_2 powder [8], its thin films [9,10], composites [11], and oxidized surface layers of biomedical titanium and Ti-alloys [12]. It has been thoroughly tested in components known for their proneness to infections, such as external fixators [13,14]. Using the biocidal activity of ROS enables prophylactic antibiotic activity and tackles host immune response, because reactive oxygen species (i.e., free hydroxyl radicals, superoxide anion radicals, and hydrogen peroxide) directly decompose organic compounds and kill bacteria

E-mail address: pezzotti@kit.ac.jp.

https://doi.org/10.1016/j.mtchem.2018.05.004
2468-5194/

by damaging their outer bacterial cell membrane [15,16]. However, the ability of TiO_2 to decompose organic compounds in bacteria becomes preponderantly activated only upon exposure to ultraviolet light, which is not the case of components embedded in the human body.

RNS, such as N_2O, NO, and $^{-}OONO$ are another type of extremely effective biocidal agents [17–20]. Significant advances in developing new NO donors to treat resistant bacteria have been reported [21,22]. However, their application in clinical practice is yet *in embryo*, because free NO donors, such as NONOates and RSNOs, are relatively unstable and prone to uncontrolled release [23]. Recent strategies to increase stability in releasing NO included their trapping into nanomaterial scaffolds or zeolites [24,25]. In a recent paper, Sahlberg Bang et al. [26] reported that an NO-donor enhanced antimicrobial effects against multidrug-resistant *Escherichia coli* when acting in combination with traditional antibiotics. Attempts were also published, which gave positive outputs in treating infected wounds and chronic infections [27,28], although cytotoxicity issues toward mammalian cells remained open as a consequence of the nano-scale size of such NO vectors [29].

In this paper, the peculiar surface chemistry of bulk Si_3N_4 bioceramic as exogenous NO donor is unfolded and its potential benefits in reducing implant-associated bacterial infections through spontaneous RNS elution are discussed. We used *in vitro* experiments on gram-positive *S. epidermidis* for validating the efficacy of this new approach and elucidating its active substance. Yet classified in the contact-killing category, the solid-state RNS approach retains the advantage of counteracting reservoirs of antibiotic-resistant bacteria. However, unlike TiO_2, which requires photocatalytic activation, it is spontaneously activated in aqueous solution. Moreover, unlike directly eluted exogenous NO, RNS eluted from solid Si_3N_4 surfaces become slowly and continuously available into the biological environment, thus providing long-term efficacy against bacterial colonies including mutants. When slowly delivered, NO radicals have also been shown to enhance differentiation and osteogenic activity of human osteoblasts [30,31].

2. Experimental procedures

Commercially available bulk Si_3N_4 bioceramic (MC$^{2®}$; Amedica Corporation Salt Lake City, UT, USA) substrates were used in this study. This biomaterial had a nominal composition of 90 wt % Si_3N_4, 6 wt% Y_2O_3, and 4 wt% Al_2O_3, the two latter phases being added for material densification during manufacturing. In the bulk sample, these additives partly reacted with the bulk Si_3N_4 grains to form an intergranular partially crystallized SiYAlON oxynitride phase. Both as-fired (rough) and polished (smooth) Si_3N_4 samples were investigated. PEEK (ASTM D6262, Ketron®PEEK 1000, Quadrant EPP USA, Inc., Reading PA, USA distributed by McMaster-Carr, Santa Fe Springs, CA, USA) and titanium alloy (ASTM F136, Ti6Al4V-ELI; Vincent Metals, Minneapolis, MN, USA) substrates were concurrently investigated as negative and positive control samples, respectively. A number of four identical disc samples (Ø12.7 × 1 mm) per each type of substrate were used for biological testing and *in situ* spectroscopic analyses. The surface topography of the substrates was quantitatively characterized by both confocal scanning laser microscopy (Laser Microscope 3D & Profile measurements, Keyence, VKx200 series, Osaka, Japan) and atomic force microscopy (AFM; MFP-3D-Bio™ equipment; Oxford Instruments Asylum Research; Santa Barbara, CA, USA). In the former method, the surface roughness, *Ra*, parameter was computed as a mean value over 36 images randomly acquired on each sample surface using a 150× magnification. AFM experiments were conducted using a) using a silicon nitride cantilever BL-AC40TS (Olympus Optical Co., Ltd., Tokyo, Japan) designed for tapping mode measurements in liquid (resonance frequency was 25 kHz in water with 0.09 N/m spring constant). The scanning rate was constantly kept at 0.5 Hz.

S. epidermidis (14990®ATCC™) were cultured in heart infusion (HI) broth (Nissui, Tokyo, Japan) at 37 °C for 18 h, and titrated by colony forming assay using brain heart infusion (BHI) agar (Nissui). After dilution with a phosphate-buffered saline (PBS) at physiological pH and ionic strength, each 100 μl of the bacterial suspension at a density of 1×10^8 CFU/ml was spread onto a BHI agar plate. The substrates, previously sterilized by UV irradiation, were stamped to the bacteria on BHI agar for inoculation, followed by incubation at 37 °C under aerobic conditions for 12, 24 and 48 h.

Samples after bacterial exposures of increasing times were screened to verify bacterial metabolism using a colorimetric assay (Microbial Viability Assay Kit-WST, Dojindo, Kumamoto, Japan). The assay employed a colorimetric indicator (WST-8), which produced a water-soluble formazan dye upon reduction in the presence of an electron mediator. The amount of generated formazan dye was directly proportional to the number of living microorganism. Solutions were analyzed using micro plate readers (EMax, Molecular Devices, Sunnyvale, CA, USA) upon collecting the optical density (OD) value related to living cells. Bacterial samples were also observed by means of a fluorescence microscope (BZ-X700; Keyence, Osaka, Japan) after exposure to Si_3N_4 or Ti-alloy substrates. For visualization, bacteria were stained with different solution: 4′,6-diamidino-2-phenylindole (DAPI), which binds to and stains blue the DNA thus imaging the nucleus location; and, Propidium Iodide (PI; Dojindo, Kumamoto, Japan), which stains red only dead bacteria.

Nitric oxide (NO) real-time activity in living bacteria was also monitored through fluorescence imaging by means of diaminofluorescein-2 diacetate (DAF-2(NO)), a membrane permeable fluorescent indicator (Goryo Chemical, Inc., Sapporo, Japan). Dye-loaded bacteria were observed *in situ* on different substrates at increasing exposure times. Dye-loaded bacteria were excited with the 488 nm of a Krypton/Argon laser, and DAF-2 fluorescence monitored *in situ* during bacterial proliferation.

In situ Raman spectra were collected on living bacteria using a highly sensitive spectroscope (LabRAM HR800, Horiba/Jobin-Yvon, Kyoto, Japan) with a 20x optical lens. The spectroscope was operated in microscopic mode using a confocal imaging capability in two dimensions. It incorporated a specially crafted holographic notch filter into the optical circuit, which enabled achieving a high spectral sensitivity. The excitation source was 532 nm with a power of 10 mW. The spectral resolution was 1.5 cm^{-1}. The Raman emission was monitored by a single monochromator connected with an air-cooled charge-coupled device (CCD) detector (Andor DV420-OE322; 1024 × 256 pixel). The acquisition time was fixed at 10 s. In time-lapse assessments, bacteria were assessed *in situ* on the ceramic substrates at increasing exposure times between 0 and 48 h. Average of ~30 spectral collections per substrate and per exposure time were assumed as characteristic of each sample. Raman spectra were deconvoluted into Gaussian-Lorentzian subbands using a commercially available software package (LabSpec 4.02, Horiba/Jobin-Yvon, Kyoto, Japan).

The unpaired Student's *t*-test was utilized for statistical analyses. A p value <0.05 was considered statistically significant and labeled with two asterisks. On the other hand, values of $p > 0.05$ were considered as statistically non-significant and labeled "*n.s.*". Standard deviations were calculated according to the general definition, namely, as the square route values of the ratio between the sum of the squared deviation of each individual set of data and the total number of measurements minus one.

3. Results

3.1. Substrate surface topography

Laser microscopy images are shown in Fig. 1(a)–(d) for Ti-alloy, PEEK, as-fired Si_3N_4, and polished Si_3N_4 substrates, respectively. The related 3D plots by AFM are given in inset to each micrograph together with surface roughness values, R_a, ± its standard deviation. The Ti-alloy (Fig. 1(a)) and PEEK (Fig. 1(b)) substrates showed different surface topography with the roughness value (and the standard deviation) of the former being about one order of magnitude smaller than that of the latter. The as-fired Si_3N_4 substrate (Fig. 1(c)) exhibited a peculiar surface topography with protruding acicular grains and a roughness in the order of few hundreds of nm (similar to that of the Ti-alloy substrate). On the other hand, the polished Si_3N_4 substrate (Fig. 1(d)) presented the smoothest surface topography among the investigated samples, with a R_a value about three times smaller than the as-fired one.

3.2. Microbial viability and fluorescence microscopy results

Fig. 2 summarizes the time-lapse results of microbial viability performed on the four different types of investigated substrate. Bacterial cell viability was probed at three different exposure times, namely 12, 24, and 48 h. After exposures of 12 h, the PEEK and Ti-alloy samples showed the highest optical density (OD) value (~1.2 with no significant statistical difference) indicating the highest number of living bacteria among all studied samples. However, while the positive control Ti-alloy substrate experienced a gradual decrease in OD value down to ~0.35 after 48 h, in the negative control PEEK substrate the OD value gradually increased with time up to ~1.4 after 48 h. Decreasing trends (with no statistical difference to each other) could be observed for both the as-fired and polished Si_3N_4 substrates. The OD values detected for these two ceramic substrates were lower (with statistical significance) than

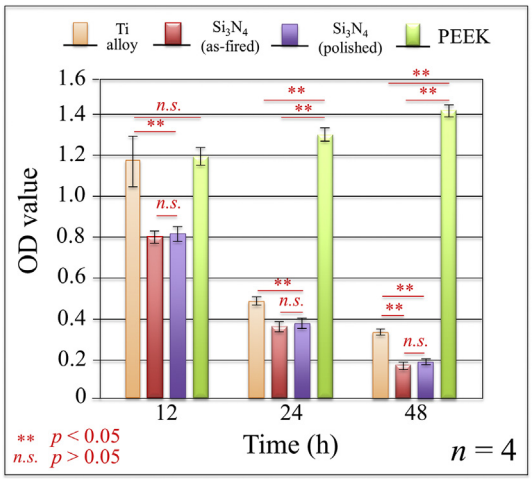

Fig. 2. Results of time-lapse experiments of microbial viability performed on four different types of substrate. Bacterial cell viability is probed after 12, 24, and 48 h.

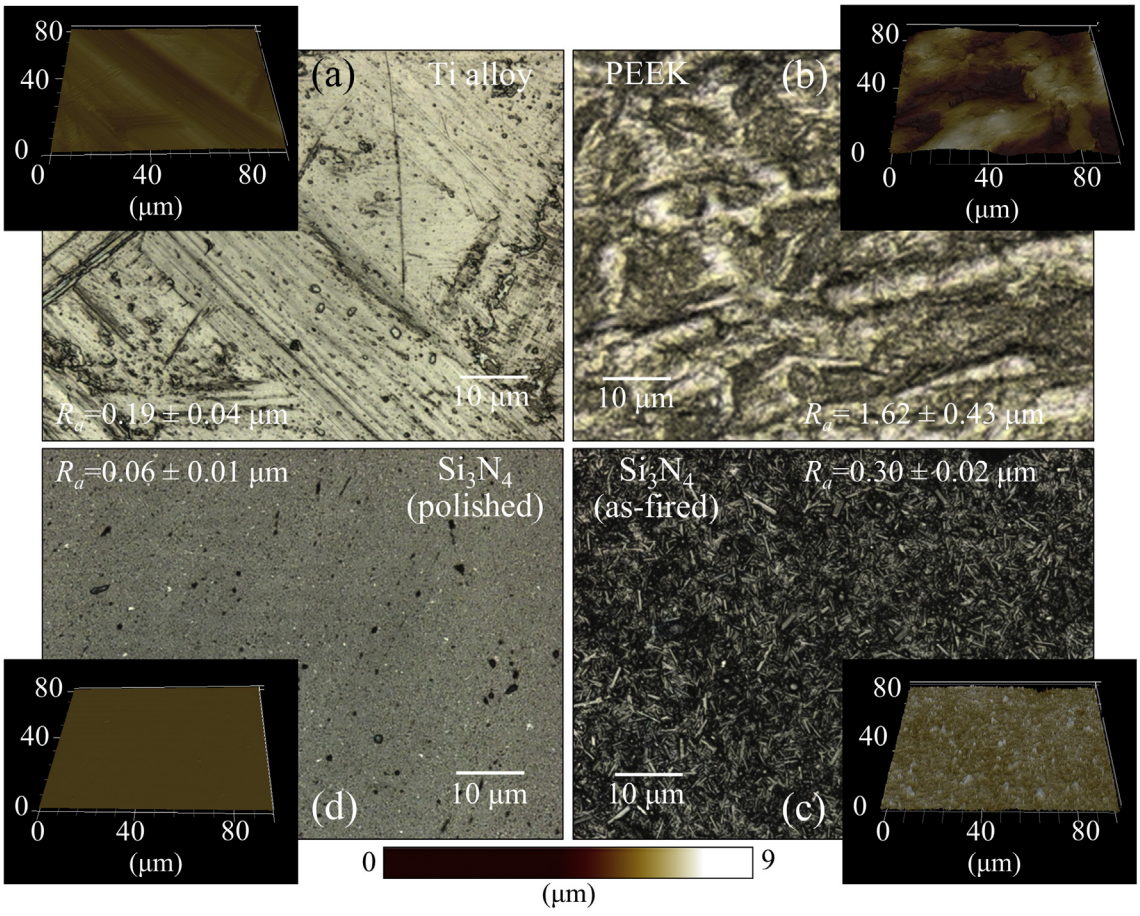

Fig. 1. Laser microscopy images of (a) Ti-alloy, (b) PEEK, (c) as-fired Si_3N_4, and (d) polished Si_3N_4 substrates before exposure to bacteria.

those of the positive control Ti-alloy substrate. OD values as low as 0.2 after 48 h exposure of *S. epidermidis* to Si_3N_4 were comparable with the background of the OD measurement (~0.15).

Fluorescence micrographs were obtained at 24 and 48 h of exposure for *S. epidermidis* on as-fired and polished Si_3N_4 substrates, after staining with 4′,6-diamidino-2-phenylindole (DAPI) and propidium iodide (PI) markers, which colored nuclei (blue) and dead bacteria (red), respectively. Results are shown in Fig. 3 (cf. labels for different samples/stains) with a constant magnification of 20x for all micrographs. Fluorescence micrographs confirmed the main output of OD assessments: for both types of silicon nitride substrate, bacterial lysis predominantly took place at >24 h and the almost totality of bacteria was dead after 48 h. However, an important difference between the as-fired and polished samples could be found in the distribution of bacteria on the substrate after 48 h. In the rough topography of the as-fired Si_3N_4 sample, bacteria showed clear signs of maturation with aggregation into colonies, which were not observed on the polished type of Si_3N_4 substrate tested under the same conditions (cf. lower set of micrographs in Fig. 3). This difference suggests a different kinetics in bacterial adhesion related to Si_3N_4 substrate topography. This point will be further discussed in the forthcoming Section 4.

Fig. 4 summarizes statistically validated results of time-lapse fluorescence spectroscopy on DAF-2(NO)-stained *S. epidermidis* on Ti-alloy, as-fired Si_3N_4, polished Si_3N_4, and PEEK substrates at 12, 24, and 48 h, exposures. A sharp rise of NO-green counting pixels could only be observed for the two Si_3N_4 substrates at the intermediate time of 24 h. This was in contrast with a nearly constant trend for NO concentration with time detected for bacteria on Ti-alloy substrate and a mild linear increase for PEEK substrate. However, such an abundant development of NO on both Si_3N_4 surfaces significantly decreased after 48 h. Bacterial metabolism naturally induces NO development in proliferating bacteria [32], which justifies the mild increasing NO trend observed for the growing *S. epidermidis* population exposed to the PEEK substrate. However, the preponderant increase in NO concentration observed for Si_3N_4 substrates under the same testing conditions suggests that NO formation was also contributed by an external supply of nitrogen species from the Si_3N_4 substrates toward the intracellular space. Such an external supply strongly alters the intrinsic metabolism of living bacteria by activating bacterial NO synthases. Fluorescence micrographs taken at 24 h and including DAPI and DAF are compared in Fig. 5 for as-fired and polished Si_3N_4 substrates (cf. labels in inset). The micrographs confirmed the

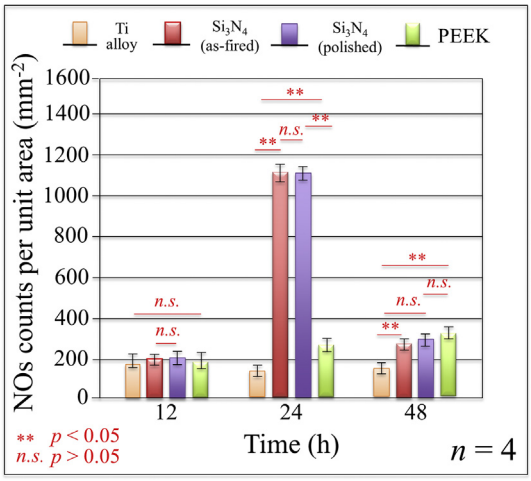

Fig. 4. Statistically validated results of time-lapse of NO concentrations on DAF-2(NO)-stained *S. epidermidis* on four different types of substrate at 12, 24, and 48 h, exposures.

morphological difference noticed in Fig. 3 with colonized bacteria only on the as-fired Si_3N_4 substrates: the rough Si_3N_4 topography allowed quicker maturation of bacteria and their successive aggregation into colonies as compared to a polished Si_3N_4 substrate.

3.3. *In situ* time-lapse Raman spectroscopic results

Fig. 6(a) shows a deconvoluted Raman spectrum (averaged over 30 spectra), which was collected *in situ* on as-cultured living *S. epidermidis* in the spectral interval between 600 and 900 cm^{-1}. In Fig. 6(b)–(d), Raman spectra are shown for *S. epidermidis* exposed for 48 h to as-fired Si_3N_4, polished Si_3N_4, and Ti-alloy substrates, respectively. The selected frequency interval displayed eight bands belonging to organic molecules from bacteria. A label number in inset is assigned to each band (cf. Table 1, in which spectral locations, physical meanings, and literature references are also specified) [33–37]. The *in situ* observation of the evolution with time of Raman bands from bacteria exposed to different substrates gave us the possibility of validating the interpretation of biological assays described in the previous sub-section and to further probe bacterial metabolism.

All the Raman spectra were normalized with respect to the strongest band in the studied interval of frequencies. Accordingly,

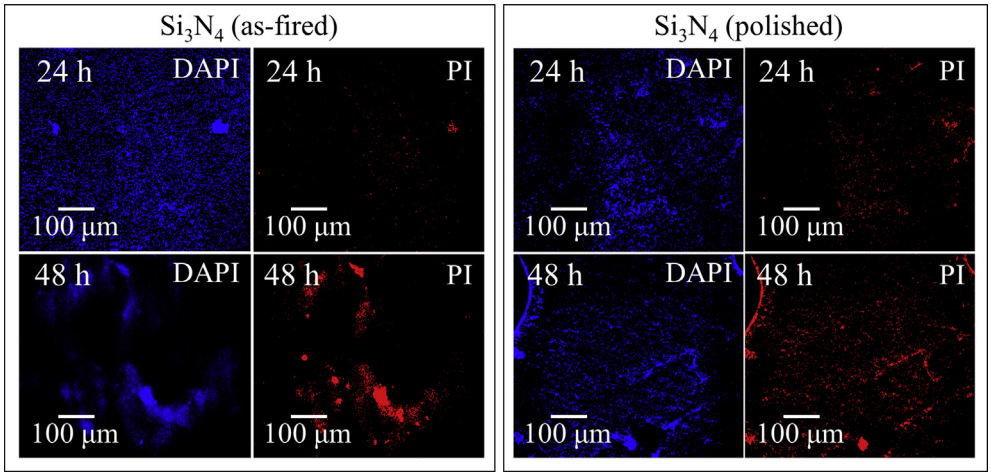

Fig. 3. 20x fluorescence micrographs at 24 and 48 h of *S. epidermidis* on as-fired and polished Si_3N_4 substrates (staining with DAPI (blue) and PI (red) markers for nuclei and dead bacteria, respectively). (For interpretation of the references to color in this figure legend, the reader is referred to the Web version of this article.)

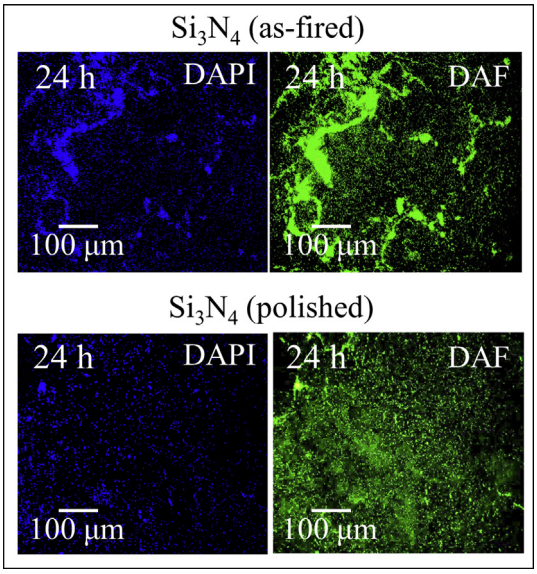

Fig. 5. Fluorescence micrographs taken at 24 h of *S. epidermidis* on as-fired and polished Si_3N_4 substrates, which include DAPI (blue) and DAF (green) to stain nuclei and NO radicals, respectively. (For interpretation of the references to color in this figure legend, the reader is referred to the Web version of this article.)

the band of spectral normalization differed for bacteria exposed to different substrates. Band 7, located at ~860 cm^{-1}, was a common reference in normalizing the spectra of as-cultured bacteria and bacteria exposed to the two Si_3N_4 substrates with topologically different surfaces. This band, which is assigned to COC 1,4 glycosidic link in carbohydrates [33], could be assumed as a probe of the external peptidoglycan side of the bacterial membrane. On the other hand, in the Raman spectrum of bacteria exposed to Ti-alloy substrates, the most intense emission arose from the DNA-related Band 2 located at ~670 cm^{-1}. This band represents ring-breathing vibrations in guanine (Gua) [35]. It belongs to a doublet with the similarly strong Band 1, which is located at ~655 cm^{-1} and arises from ring vibrations in poly-deoxyadenosine (dAdo) [34].

Conversely, the most dramatic changes in the Raman spectrum of *S. epidermidis* after 48 h exposure to the polished Si_3N_4 substrate consisted in the complete disappearance of Bands 1 (ring dAdo), 2 (ring Gua), and 5 (at 655, 670, and 782 cm^{-1}, respectively) (Fig. 6(c)), whereas a conspicuously unchanged Raman emission from the membrane carbohydrate Band 7 could be observed as compared to the as-cultured bacterial sample. Band 5 belongs to

Table 1
Assignments and physical origins of the Raman bands in Fig. 6.

Band	Assignment	Frequency (cm^{-1})	Reference
1	Ring vibrations in poly-deoxyadenosine C-C-C out-of-plane bending in xanthine	650	[34, 58]
2	Ring breathing in guanine	670	[35]
3	Adenine DNA & phosphatidylserine	730	[35]
4	Ring breathing DNA	746	[35]
5	Phosphodiester stretching	782	[36]
6	Out-of-plane ring breathing in DNA	830	[37]
7	COC 1,4 glycosidic link in carbohydrates	860	[33]
8	C-C stretching in protein backbone	896	[37]

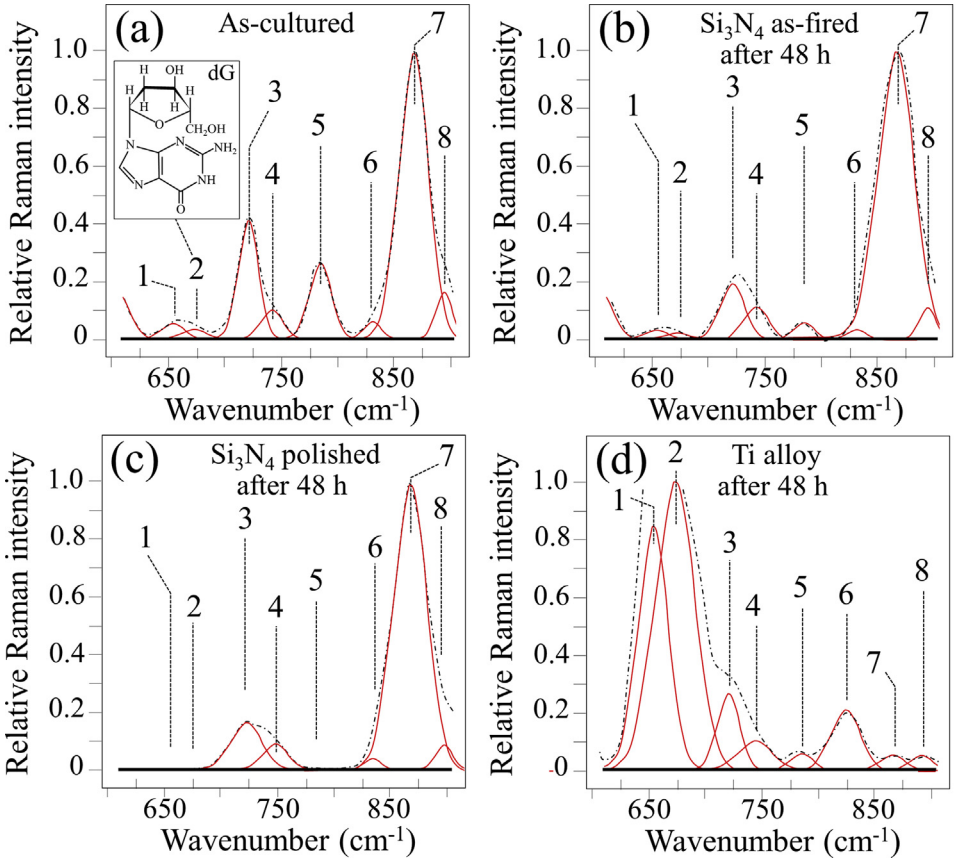

Fig. 6. Deconvoluted Raman spectra (averaged over 30 measurements) collected *in situ* on (a) as-cultured living *S. epidermidis* and *S. epidermidis* exposed for 48 h to (b) as-fired Si_3N_4, (c) polished Si_3N_4, and (d) Ti-alloy substrates. As-cultured bacteria were not yet exposed to the Si_3N_4 substrate. The labeling numbers in inset refer to Table 1.

the internal (phospholipid) membrane of gram-positive bacteria and represents stretching vibrations in phosphodiesters [36]. A similar but less pronounced decrease could be observed for DNA-related bands for bacteria exposed to the as-fired Si_3N_4 substrate (Fig. 6(b)). Interestingly, Band 3 at ~730 cm^{-1}, which also belongs to DNA (adenine) and phosphatidylserine [35], also showed intensity decrease and broadening upon exposure similar for both polished and as-fired Si_3N_4 substrates.

A different trend could be observed in the Raman spectrum of bacteria exposed to the Ti-alloy substrate (Fig. 6(d)). Also in this case, bold variations could be observed in DNA-related Raman emissions Bands 1 and 2, but with an opposite (increasing) trend with respect to as-cultured bacteria (cf. Fig. 6(a) and (d)). Band 2 was also found shifted by ~7 cm^{-1} toward lower frequencies as compared to unexposed bacteria. The additional DNA-related bands in the Raman spectrum (Bands 3, 4; cf. Table 1) decreased in intensity and partly broadened, while Band 6 (out-of-plane ring breathing in DNA) [37] increased consistently with the trend of the other ring-breathing-related bands (i.e., Bands 1 and 2). However, the most striking feature in the Raman spectrum of *S. epidermidis* exposed for 48 h to Ti-alloy substrates was the almost complete disappearance of Band 7 (membrane carbohydrates) as compared to as-cultured bacteria. This feature could be interpreted as the fingerprint of degradation of the carbohydrates constituting the external peptidoglycan structure of the membrane, as discussed in the next section.

The results of time-lapse *in-situ* Raman experiments are summarized in Fig. 7. In section (a) of this figure, the relative Raman intensity I_5/I_7 is plotted as a function of exposure time for Raman spectra recorded on bacteria exposed to both as-fired and polished Si_3N_4 substrates in comparison with as-cultured bacteria. This ratio could be assumed as a measure of DNA degradation, the lower the intensity the more damaged the DNA structure. The plot in Fig. 7(a) shows that a threshold time exists before DNA degradation abruptly starts in bacteria exposed to Si_3N_4 substrates, and that such a threshold depends on the roughness of the substrate; the rougher the surface the longer the time threshold. The threshold time for DNA degradation on as-fired Si_3N_4 was about twice that observed for the polished Si_3N_4 substrate. Fig. 7(b) gives the trend with exposure time of another spectroscopic parameter that comparatively describes the rate of degradation for DNA vs. membrane, namely, the ratio, $(I_1+I_2+I_3+I_4+I_6)/(I_5+I_7)$, between the cumulative intensity of bands related to DNA vs. that of bands emitted from the membrane. This latter parameter shows that bacteria exposed to the Ti-alloy substrate predominantly suffered from external membrane degradation (peptidoglycan wall), and that such degradation started from the very early stage of exposure and rose exponentially with time. On the other hand, both as-fired and polished Si_3N_4 substrates affected bacteria metabolism by predominantly damaging the DNA structure, while the peptidoglycan structure of their membrane was hardly altered. Both membrane and DNA degradation processes ultimately led to bacterial lysis on the respective substrates, as demonstrated by the OD data given in Fig. 2. However, they were different in their nature and kinetics. We shall discuss hereafter the salient chemical details of the respective degradation processes.

4. Discussion

4.1. Mechanisms of bacterial lysis induced by substrate-generated free radicals

In aqueous solution, Si_3N_4 undergoes dissociation of the Si-N covalent bond at its surface. Following homolytic cleavage of the bond, a new equilibrium is found with silicon dioxide (SiO_2) and ammonia (NH_3) formation at the bioceramic surface and in the neighboring aqueous environment, respectively. Subsequently, the newly formed silicon oxide clusters further react with water to form surface silanols, whose dissociation (together with that of surface amine sites) generates free electrons and oxygen/nitrogen free radicals [38–40]. Fig. 8(a) summarizes the off-stoichiometric chemical reactions, which ultimately lead to the huge formation of NO radicals experimentally observed at intermediate exposure times to Si_3N_4 substrates (cf. Fig. 4). The scheme shown in Fig. 8(a) is explained in the following. Dissociation of surface silanols is the starting point for the formation of superoxide radicals, such as $(\equiv Si-O^{\bullet})$ and $(\equiv Si-O_2^{\bullet})$. Concurrently, unpaired electrons react with adsorbed O_2 on the Si_3N_4 surface to yield $O_2^{\bullet-}$ radical anions and other highly oxidative protonated radicals. In contact with bacteria, NH_3 first oxidizes into hydroxylamine NH_2OH (ammonia monooxygenase) [41] in the presence of superoxide radicals and by exploiting two free electrons from ammonia. An additional reductant contribution to reduce the second O atom forming H_2O leads to further oxidation of NH_2OH into nitrite (NO_2^-) through a process of

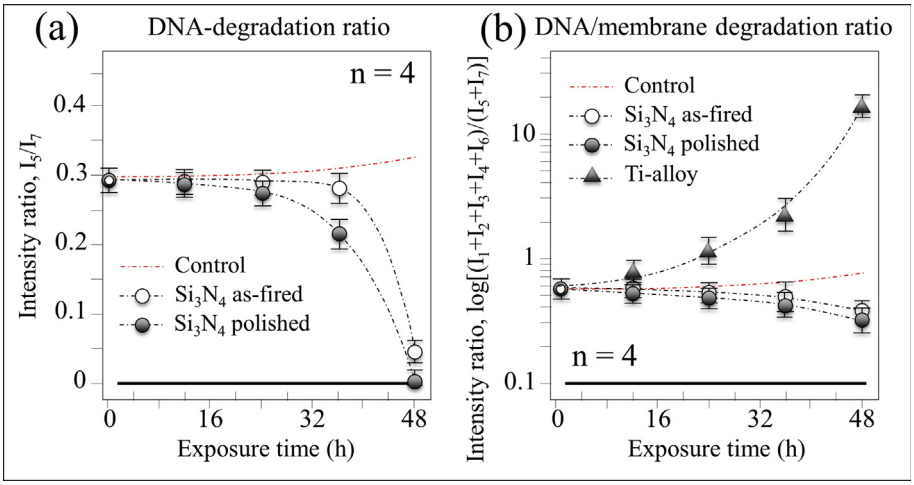

Fig. 7. Summary of time-lapse *in-situ* Raman experiments: (a) the relative Raman intensity I_5/I_7 and (b) the intensity ratio, $(I_1+I_2+I_3+I_4+I_6)/(I_5+I_7)$, between the cumulative intensity of bands related to DNA vs. bands emitted from the membrane are plotted as a function of exposure time for bacteria on as-fired and polished Si_3N_4 substrates in comparison with as-cultured bacteria.

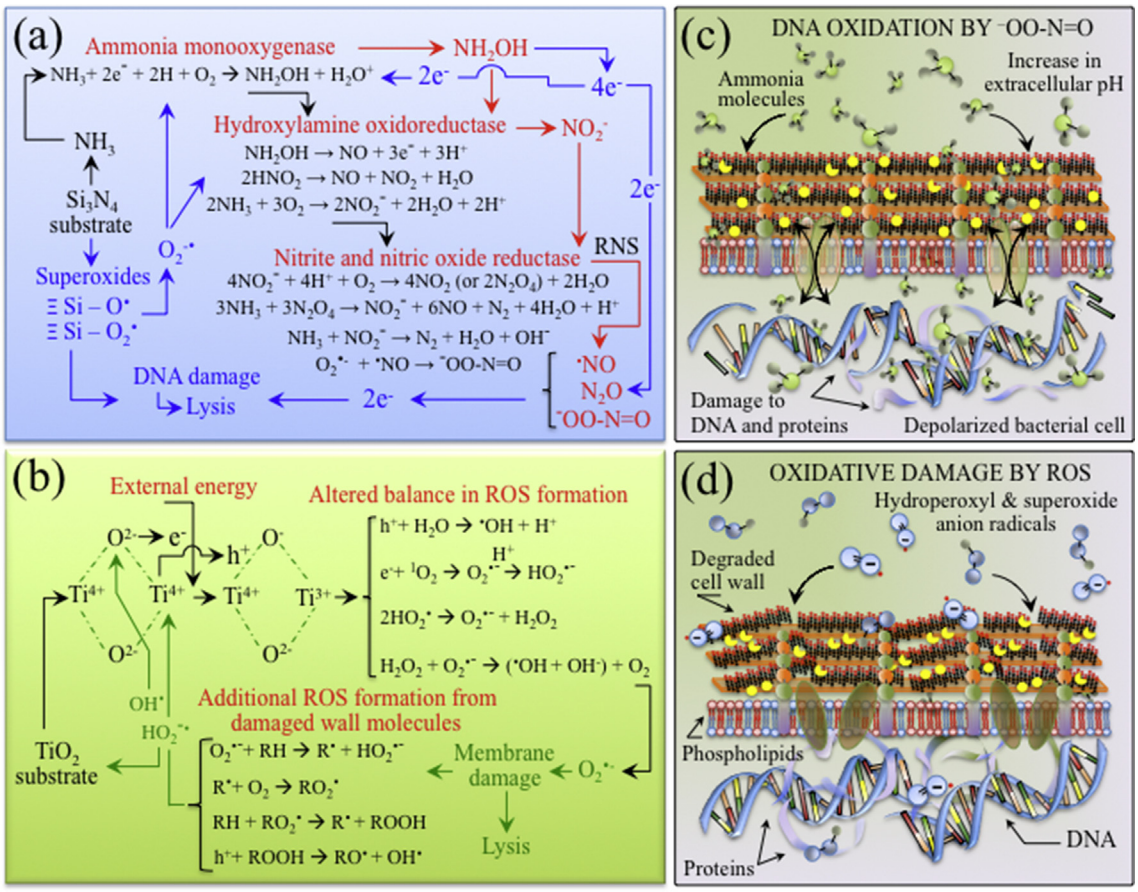

Fig. 8. The cascade of off-stoichiometric chemical events leading to the formation of RNS (a) and ROS (b) at the interface between different substrates and bacteria. In (c) and (d), schematic drafts of the *S. epidermidis* DNA structure and external peptidoglycan membrane under the attack of free radicals from Si_3N_4 and TiO_2, respectively.

hydroxylamine oxidoreductase. This latter process releases four electrons, two of which sustain further ammonia oxidation, while the remaining two electrons become available to bacterial metabolism and generation of proton gradients [41]. Relevant to bacterial lysis are also some secondary (highly reactive and oxidative) gaseous products of ammonia oxidation, such as NO_2, NO, and $^{-}OONO$ [42]. The cascade of off-stoichiometric chemical events (i.e., monooxygenase, oxidoreductase, and the formation of gaseous oxidizing by-products), as shown in Fig. 8(a), is peculiar to Si_3N_4 surfaces in aqueous environment. It originates from ammonia and silanol formation [43–45], and abundantly produces RNS at the interface between Si_3N_4 substrate and bacteria.

Jennison et al. [46] have previously shown that TiO_2 layers on titanium and Ti-alloys possess some antibacterial efficacy even in the absence of photocatalytic reactions. Following that study, advanced engineering technologies of surface ceramic conversion have been developed and applied to self-drilling Ti6Al4V external fixation pins to improve their performance in terms of antibacterial properties [47]. This study confirms those recent reports and adds some physical chemistry details to the known free-radical effect of the TiO_2 surface layer in counteracting colonization of bacterial strains. Effective TiO_2 thicknesses for triggering antibacterial effects were reported to be between 3 and 20 nm [48–50]. The origin of the antibacterial effect of TiO_2 resides in the formation of TiOH metastable intermediate. This process is greatly enhanced by ultraviolet light irradiation, but it partly takes place also in dark environment [51]. Accordingly, TiO_2 generates charges with the formation of oxygen vacancies reducing Ti^{4+} to Ti^{3+} [52]. Fig. 8(b) summarizes the (oxygen) radical chemistry pathway leading to the antibacterial properties of a TiO_2 layer. The generation of electrons, e^{-}, and holes, h^{+}, leads to dissociative chemisorption of water from the environment, which releases reactive oxygen species (ROS) such as hydroxyl radicals ($^{\bullet}OH$), superoxide ($O_2^{\bullet-}$), singlet oxygen ($^1O_2$), and hydrogen peroxide (H_2O_2) from the TiO_2 surface [53]. As specifically explained in Fig. 8(b), the generated h^{+} and e^{-} are precursors to the formation of $^{\bullet}OH$ and $O_2^{\bullet-}$ radicals, which in turn recombine with free electrons to form $HO_2^{\bullet-}$ and H_2O_2. Successively, the highly oxidative radicals thus formed interact with the chemical species contained in the peptidoglycan membrane layer of gram-positive bacteria, R, to produce degraded species $R^{\bullet}$, $RO^{\bullet}$, $RO_2^{\bullet}$, and additional ROS. The most acute effects on bacteria are induced by $^{\bullet}OH$ and $^1O_2$ species, while $O_2^{\bullet-}$ and H_2O_2 radicals are much less reactive since they can be detoxified by endogenous (both enzymatic and non-enzymatic) antioxidants. On the other hand, no enzyme can detoxify $^{\bullet}OH$ and $^1O_2$ radicals. This circumstance renders those radicals acutely lethal [54]. Self-propagating chain reactions are thus created, which ultimately leads to destruction of the bacterial membrane.

4.2. *Metabolic fingerprints in the bacteria Raman spectra*

In this subsection, we look for spectroscopic fingerprints in the attempt to substantiate the different bacterial lysis mechanisms induced by RNS and ROS on Si_3N_4 and oxidized TiO_2 substrates, respectively. DNA emits marker Raman bands whose variations directly reveal breakages or other conformational changes in the double-helix structure [55]. Structural changes in the primary structure of DNA also reflect into spectral changes of breathing

modes of its ring structures (e.g., Gua pyrimidine-imidazole ring drafted in inset to Fig. 6(a)). Specifically, ring vibrations reveal the presence of DNA breakages and bond alterations. DNA oxidation occurs upon reaction with reactive nitrogen species (e.g., HNO_2 or ONOOH) most readily at guanine sites, due to the high oxidation potential of this base as compared to others (e.g., adenine). In the oxidative process of oxidative deamination, NH_2 groups are replaced with OH groups (upon which guanine transforms into xanthine) [56]. Ring vibrations are also affected by metal ions, which readily coordinate at guanine N-sites. Alterations in ring bands are general to many different metallic ions, although it is hardly possible to single out the nature of a specific metal ion from the observed vibrational variations [57]. In this study, we have observed disappearance and strong enhancement (with spectral shift from 675 to 668 cm^{-1}) of the ring breathing guanine Band 2 upon exposing bacteria to Si_3N_4 and Ti-alloy, respectively. These observations suggest the occurrence of DNA oxidation to form deaminated guanine and newly formed metal coordination sites (Ti or Al or V ions) at specific guanine sites in the former and latter case, respectively.

Peroxynitrite, which forms from the reaction of nitric oxide and superoxide radical anions (cf. Fig. 8(a)), initiates DNA damage together with other RNS eluted from the Si_3N_4 substrates. Rapid protonation in the endocytotical space leads to the formation of peroxynitrous acid, ONOOH, a strong nitrating agent for side chains in proteins. Peroxynitrous acid eventually reacts with deoxyribose backbones and causes single- and double-strand breaks, together with nitration or deamination of guanine and, subsequently, of other DNA bases. In our Raman data (cf. Fig. 6(a)–(c)), a fingerprint for preferential degradation of guanine was the disappearance of the guanine Band 2, while the intensity of the adenine Band 3 showed a smaller reduction when bacteria were exposed to Si_3N_4 substrates. However, the disappearance of the guanine Band 2 at ~670 cm^{-1} from the Raman spectrum was not accompanied by an increase of the main xanthine band expected at ~650 cm^{-1} (i.e., overlapping Band 1) [58]. This could be explained with mispairing of the newly generated xanthine, resulting in nuclear base transversion mutations of nucleic acids. Then, as deaminative damage spreads to other DNA forms, strand breakage occurs as a result of alkylperoxynitrites formation from the reaction of nitric oxide with alkylperoxy radicals. NO is a gaseous lipophilic molecule, which can easily penetrate the bacterial membrane. Accordingly, DNA damage in bacteria exposed to Si_3N_4 substrates can take place *before* any significant damage occurs to the external membrane (Fig. 8(c)). Note that lipids of the internal membrane are also damaged, as confirmed by the disappearance of Band 5 in Fig. 6(c)).

The formation of metal coordination sites at the pyrimidine-imidazole ring of guanine nucleoside, dG (O and NH sites; cf. draft in inset to Fig. 6(a)), is key in the exposure of bacteria to oxidized Ti-alloy substrates. A Raman study by Jang [59] reported intensity enhancement and shift to lower frequencies for guanine ring-breathing (as well as C-N and C=N stretching) bands upon exposure of DNA to metallic surfaces. Such an enhancement was explained with a strong and direct interaction between dG and metal ions, which affects the neighboring C=O carbonyl group (cf. draft in inset to Fig. 6(a)). Such an interaction restructures the ring charge and alters the Raman spectrum with characteristics similar to those observed for Band 2 in Fig. 6(d). The enhancement of Band 1, which was another peculiarity of bacteria exposed to Ti-alloy substrates, could instead be interpreted as a metabolic effect of xanthine accumulation, although also an increase in dAdo cannot be ruled out. As mentioned above, the strongest Raman band of xanthine appears at ~650 cm^{-1} (C-C-C out-of-plane bending vibrations) [58] and overlaps the dAdo ring vibration labeled as Band 1 in the as-cultured bacteria sample. The suggested scenario for the interaction between *S. epidermidis* and Ti-alloy substrate foresees the produced ROS exceeding the bacterial antioxidant capacity. While metal ions inhibit polymerization of glycan saccharide chains, ROS debunk the external peptidoglycan membrane (Fig. 8(d)) [60]. Under oxidative stress, bacteria undergo metabolically driven guanine deamination. Adenosine enrichment has been reported for several bacterial pathogens under metabolic stress conditions [61]. Moreover, excess in xanthine is also the consequence of a metabolic reaction by bacteria, which inactivate xanthine oxidase under oxidative stress by $O_2^{\bullet -}$ radicals [54].

4.3. Importance of Si_3N_4 as a solid-state NO donor

S. epidermidis is the causative agent most frequently involved with infections of medical devices, including peripheral or central intravenous catheters, prosthetic joint, and prosthetic valves [62]. Moreover, this bacterium is one of the most significant species among methicillin-resistant coagulase negative *staphylococci* encountered in the clinical practice [62]. Approximately 80–90% of *S. epidermidis* strains isolated from patients with nosocomial infections carried the *mec*A gene, which enables this bacterium to show increasing resistance to different groups of antibiotics [63]. This study shows that N free radicals and Si superoxides, which are spontaneously eluted from Si_3N_4 substrates in aqueous environment, operate in concert to damage DNA and internal membrane species in gram-positive *S. epidermidis*. The diverse pathways through which NO exerts its antibacterial effects would require multiple and simultaneous mutations to occur for bacteria to survive. This circumstance hinders the development of resistance, which in the case of exogenous NO from Si_3N_4 substrates could be regarded as a low probability event. In support of this argument, a study by Privett et al. [64] could be mentioned, in which the potential bacterial resistance of NO-releasing silica nanoparticles was evaluated for a number of different bacteria. The bacterial strains were unable to develop resistance toward NO release. Si_3N_4 bioceramic substrates maintain the advantages of NO-releasing agents but avoid the negative implications related to the cytotoxicity of nanoparticles. In substance, using Si_3N_4 in bulk or as a coating to metallic components can provide long-term protection against infections and solve issues related to antibiotic resistance of bacteria carrying the *mecA* gene.

While we report here about the *intrinsic* functionality of a non-oxide bioceramic in stimulating NO lysis in bacteria, we are aware that bulk polymers have also been used as *extrinsic* NO donors through incorporation of *S*-nitrosothiols to form hydrogels and blended solid films [65,66]. A comprehensive review on NO generating/releasing materials has recently been published by Liang et al. [67] In an earlier paper [68], covalently attached SNO groups to the polymer backbone were obtained through a condensation reaction of diols (ethylene glycol and PEG) with mercaptosuccinic acid, followed by the S-nitrosation of the SH groups by a gaseous NO/O_2 mixture. Polynitrosated polyesters were found capable to sustain NO release for >20 h at physiological temperature. One main advantage of intrinsic solid-state NO generators, such as Si_3N_4, might be a significant extension in time of the donor capacity as compared to “chemically charged” polymers, which will unavoidably reach exhaustion because of their extrinsic nature. In order to substantiate such a potential advantage for the solid-state ceramic donor, future antibacterial experiments on Si_3N_4 should be performed using polymeric NO donors as positive controls.

Another important issue in dealing with NO donors is the dose effect, which directly relates to toxicity issues in the human body [69]. A main item that researchers have long sought in this field is the possibility to control the rate and the amount of released NO:

the quantities delivered should be sufficient to achieve the desired physiological effect (i.e., the antibacterial function in the case of the present investigation), yet they should cause minimal side effects (i.e., cell damage in this case). For example, functionalized dendrimers, after being conjugated with diazeniumdiolates, have been shown to be advantageous over other NO carriers in terms of stability, storage capacity, and NO elution lifetime [70,71]. However, an inherent toxicity against mammalian cells yet represents the main issue in most dendritic constructs [72–74]. Accordingly, strategies to counteract an excess of NO delivery, which could be deleterious for biological systems, have been discussed in details as a main issue in the synthesis of NO donors [75]. Sun et al. [76] proved the superior antibacterial activity of a variety of functionalized dendrimers in comparison with their respective precursors (i.e., non NO-releasing dendrimers) against Gram-negative *Pseudomonas aeruginosa*, standard and antibiotic-resistant (MRSA) Gram-positive *Staphylococcus aureus*. The NO bactericidal activity was attributed to NO byproducts such as peroxynitrite ($ONOO^-$) and dinitrogen trioxide (N_2O_3) as agents of oxidative and nitrosative stress. Interestingly, those authors also reported about a range of concentrations for the NO-release process and disclosed some optimized materials, which exhibited minimal toxicity to fibroblast cells at bactericidal concentrations. The possibility to find a range of (low) NO concentrations that promotes cell proliferations while providing bactericidal effects has elegantly been discussed by Napoli et al. [77] As cellular responses are differentially regulated by specific NO concentrations, low concentrations in the pico- to nano-molar range generally promote cell proliferation, while being toxic to most of the bacterial strains. In this study, we only obtained a qualitative estimate of NO concentration in the tested bacteria through DAF-2(NO) tests. However, our preliminary assessments of NH_3 elution from Si_3N_4 powder in aqueous solution (at physiological pH) showed concentrations in the range of the nM. NH_3 concentrations measured on solid Si_3N_4 substrates are expected to be smaller than in the case of powder samples. Moreover, our previous *in vitro* studies of both osteosarcoma and mesenchymal cells on Si_3N_4 substrates revealed significantly enhanced cell proliferation and osteogenic activity in comparison with other ceramic, metallic and polymeric biomaterials [31,78]. This experimental evidence can be considered a further confirmation that the NO production at the surface of a Si_3N_4 substrate indeed lies in the safe range for mammalian cells.

Finally, this study contributes to clarify some yet unproven aspects of kinetics and mechanisms of bacterial lysis by ROS and RNS. The ROS antibacterial effect on TiO_2 substrates has long been explained in terms of wettability change (i.e., bacteria with hydrophobic surface properties like *S. epidermidis* adhere preferentially to hydrophobic surfaces) [51,79,80]. Conversely, we clearly substantiate here an antibacterial ROS effect of chemical nature, which is operative on the external peptidoglycan membrane. In a recently published study on Si_3N_4 bioceramics, Ishikawa et al. [81] proposed that a Si_3N_4 surface with nano-scale roughness could experience better antibacterial properties than a smooth one with exactly the same chemical composition and higher wettability [81]. The authors of this latter study invoked a "nanotopography effect" to explain their data according to an inhibition of the initial attachment of bacteria to the biomaterial surface. They eventually mentioned also the release of nitrogen as a concurrent effect with explicitly referring to Ref. 20. However, such a release was interpreted as an "effective deterrent in the attachment" of bacteria and the effect defined as a "mechanistic" rather than a chemical one, thus ignoring the chemical action of RNS on bacterial DNA. It should be noted that the Si_3N_4 materials examined by Ishikawa et al. [81] are the same as those used in this study. The presence of oxide additives stemming at the grain boundaries of Si_3N_4 (i.e., covering like a "carpet" the as-fired surface) might be the reason why the topography and higher surface area associated with as-fired in comparison to polished samples did not enhance the chemical effect in this study. We believe that a direct exposure of the bulk Si_3N_4 lattice to aqueous environment, which substantially occurs on the polished surface, is necessary to trigger the cleavage of Si-N bonds, thus allowing ammonia elution and the successive cascade of chemical reactions described in Fig. 8(a).

Note also that the protocol adopted in this study was different from the one adopted in Ref. 81; the present one not only exposed bacteria directly to bulk S-N bonds (i.e., in the case of the polished Si_3N_4 surface), but it was also designed "to force" the bacteria to remain on the substrate rather than just examining their natural propensity to adhere to it (i.e., as done in Ref. 81). This different procedure gave us the opportunity to unfold the powerful and efficient role of RNS chemistry in the antibacterial action of Si_3N_4 substrates. We believe that the surface chemistry of Si_3N_4 with its efficient kinetics is a unique phenomenon in biomaterials science, which could provide technological breakthroughs in a number of different fields of technological interest.

5. Conclusion

The main outputs of this study can be summarized, as follows:

(i) RNS developed at the interface between Si_3N_4 substrates and *S. epidermidis* in aqueous environment. A spike in NO concentration was directly monitored in living bacteria after 24 h exposure to Si_3N_4 substrates, which coincided with the beginning of DNA degradation observed by *in situ* Raman spectroscopy.

(ii) RNS developed on Si_3N_4 substrates were more efficient in inducing bacterial lysis than ROS developed on TiO_2. RNS directly attacked DNA and lipid structures, while ROS preferentially debunked the external peptidoglycan membrane.

(iii) Chemical in nature, the antimicrobial properties of Si_3N_4 were scarcely affected by the topography of the substrate surface. However, rough Si_3N_4 substrates were slightly less efficient in obstructing bacterial aggregation into colonies as compared to polished Si_3N_4 substrates.

The present findings pave the way to a promising antibacterial strategy through the use of bulk Si_3N_4 or Si_3N_4-coated components in biomedical implants. Functioning as a spontaneous NO donor, the Si_3N_4 surface provides a slow and constant release of such a potent bactericidal agent. The common characteristic of membrane permeability by gaseous N species makes this antibacterial approach viable for a wide spectrum of gram-positive and gram-negative bacteria. Moreover, the diverse mechanisms and multiple pathways of NO antibacterial effect would require multiple simultaneous mutations for bacterial resistance to be developed. Starting from the spectroscopic evidences given in this paper, further studies are presently ongoing to achieve a full clarification of the antibacterial mechanism(s) operative in different bacterial strains. Further studies should also be performed with tailored protocols to secure solid evidence through *in vivo* validations.

Data availability statement

The raw/processed data required to reproduce these findings cannot be shared at this time as the data also forms part of an ongoing study. Furthermore, the materials used are protected by patents and cannot be disclosed at this time.

Additional information – financial interests

Giuseppe Pezzotti is a consultant to Amedica Corporation which provided the samples used in this work.

References

[1] M. Zaborowska, K. Welch, R. Branemark, P. Khalilpour, H. Engqvist, P. Thomsen, M. Trobos, Bacteria-material surface interactions: methodological development for the assessment of implant surface induced antibacterial effects, J. Biomed. Mater. Res. B: Appl. Biomater. 103 (2014) 179–187.

[2] V. Alt, A. Bitschnau, J. Osterling, A. Sewing, C. Meyer, R. Kraus, S.A. Meissner, S. Wenisch, E. Domann, R. Schnettler, The effects of combined gentamicin-hydroxyapatite coating for cementless joint prostheses on the reduction of infection rates in a rabbit infection prophylaxis model, Biomaterials 27 (2006) 4627–4634.

[3] G. Schmidmaier, M. Lucke, B. Wildemann, N.P. Haas, M. Raschke, Prophylaxis and treatment of implant-related infections by antibiotic-coated implants: a review, Injury 37 (2006) S105–S112.

[4] J. Fei, G.D. Liu, C.J. Pan, J.Y. Chen, Y.G. Zhou, S.H. Xiao, Y. Wang, H.J. Yu, Preparation, release profiles and antibacterial properties of vancomycin-loaded Ca-P coating titanium alloy plate, J. Mater. Sci. Mater. Med. 22 (2011) 989–995.

[5] D. Neut, R.J. Dijkstra, J.I. Thompson, H.C. van der Mei, H.J. Busscher, A gentamicin-releasing coating for cementless hip prostheses - longitudinal evaluation of efficacy using in vitro bio-optical imaging and its wide-spectrum antibacterial efficacy, J. Biomed. Mater. Res. A 100 (2012) 3220–3226.

[6] V. Antoci Jr., S.B. King, B. Jose, J. Parvizi, A.R. Zeiger, E. Wickstrom, T.A. Freeman, R.J. Composto, P. Ducheyne, I.M. Shapiro, N.J. Hickok, C.S. Adams, Vancomycin covalently bonded to titanium alloy prevents bacterial colonization, J. Orthop. Res. 25 (2007) 858–866.

[7] D. Shchukin, H. Mohwald, Materials science. A coat of many functions, Science 341 (2013) 1458–1459.

[8] T. Matsunaga, R. Tomoda, T. Nakajima, H. Wake, Photoelectrochemical sterilization of microbial cells by semiconductor powders, FEMS Microbiol. Lett. 29 (1985) 211–214.

[9] T. Verdier, M. Coutand, A. Bertron, C. Roques, Antivacterial activity of TiO_2 photocatalyst alone or in coatings on E. coli: the influence of methodological aspects,, Coatings 4 (2014) 670–686.

[10] Y. Kikuchi, K. Sunada, T. Iyoda, K. Hashimoto, A. Fujishima, Photocatalytic bactericidal effect of TiO_2 thin films: dynamic view of the active oxygen species responsible for the effect, J. Photochem. Photobiol. Chem. 106 (1997) 51–56.

[11] A. Kubacka, M. Suarez Diez, D. Rojo, R. Bargiela, S. Ciordia, I. Zapico, J.P. Albar, C. Barbas, V.A.P. Martins dos Santos, M. Fernandez-Garcia, M. Ferrer, Understanding the antimicrobial mechanism of TiO_2-based nanocomposite films in a pathogenic bacterium, 4134 (9 pages), Sci. Rep. 4 (2014).

[12] L. Zhao, P.K. Chu, Y. Zhang, Z. Wu, Antibacterial coatings on titanium implants, J. Biomed. Mater. Res. B: Appl. Biomater. 91B (2009) 470–480.

[13] H. Koseki, T. Asahara, T. Shida, I. Yoda, H. Horiuchi, K. Baba, M. Osaki, Clinical and histomorphometrical study on titanium dioxide-coated external fixation pins, Int. J. Nanomed. 8 (2013) 593–599.

[14] M. Haenle, A. Fritsche, C. Zietz, R. Bader, F. Heidenau, W. Mittelmeier, H. Gollwitzer, An extended spectrum bactericidal titanium dioxide (TiO_2) coating for metallic implants: *In vitro* effectiveness against MRSA and mechanical properties, J. Mater. Sci. Mater. Med. 22 (2011) 381–387.

[15] P.C. Maness, S. Smolinski, D.M. Blake, Z. Huang, E.J. Wolfrum, W.A. Jacoby, Bactericidal activity of photocatalytic TiO_2 reaction: toward an understanding of its killing mechanism, Appl. Environ. Microbiol. 65 (1999) 4094–4098.

[16] M. Bekbolet, C.V. Araz, Inactivation of *Escherichia coli* by photocatalytic oxidation, Chemosphere 32 (1996) 959–965.

[17] F.C. Fang, Perspectives series: host/pathogen interactions. Mechanisms of nitric oxide-related antimicrobial activity, J. Clin. Invest. 99 (1997) 2818–2825.

[18] I. Sulemankhil, J.G. Ganopolsky, C.A. Dieni, A.F. Dan, M.L. Jones, S. Prakash, Prevention and treatment of virulent bacterial biofilms with an enzymatic nitric oxide-releasing dressing, Antimicrob. Agents Chemother. 56 (2012) 6095–6103.

[19] A.B. Seabra, M.T. Pelegrino, P.S. Haddad, Can nitric oxide overcome bacterial resistance to antibiotics? in: K. Kon, M. Rai (Eds.), Antibiotic Resistance: Mechanisms and New Antimicrobial Approaches Academic Press, London, UK, 2016, pp. 187–204.

[20] G. Pezzotti, R.M. Bock, B.J. McEntire, E. Jones, M. Boffelli, W. Zhu, G. Baggio, F. Boschetto, L. Puppulin, T. Adachi, T. Yamamoto, N. Kanamura, Y. Marunaka, B.S. Bal, Silicon nitride bioceramics induce chemically driven lysis in *Porphyromonas gingivalis*, Langmuir 32 (2016) 3024–3035.

[21] J. Jones-Carson, J.R. Laughlin, A.L. Stewart, M.I. Voskuil, A. Vazquez-Torres, Nitric oxide-dependent killing of aerobic, anaerobic and persistent *Burkholderia pseudomallei*, Nitric Oxide 27 (2012) 25–31.

[22] H. Kishikawa, A. Ebberyd, U. Romling, A. Brauner, P. Luthje, J.O. Lundberg, E. Weitzberg, Control of pathogen growth and biofilm formation using a urinary catheter that release antimicrobial nitrogen oxides, Free Radic. Biol. Med. 65 (2013) 1257–1264.

[23] M.G. de Oliveira, S.M. Shishido, A.B. Seabra, N.H. Morgon, Thermal stability of primary *S*-nitrosothiols: roles of autocatalysis and structural effects on the rate of nitric oxide release, J. Phys. Chem. A 106 (2002) 8963–8970.

[24] G. Han, L.R. Martinez, M. Radu Mihu, A.J. Friedman, J.M. Friedman, J.D. Nosanchuk, Nitric oxide releasing nanoparticles are therapeutic for *Staphylococcus aureus* abscesses in a murine model of infection, e7804 (7 pages), PLoS One 4 (2009).

[25] P.S. Wheatley, A.C. McKinlay, R.E. Morris, A comparison of zeolites and Metal Organic Frameworks as storage and deliveryvehicles for biologically active nitric oxide, Stud. Surf. Sci. Catal. 174A (2008) 441–446.

[26] C. Sahlberg Bang, A. Kinnunen, M. Karlsson, A. Önnberg, B. Söderquist, K. Persson, The antibacterial effect of nitric oxide against ESBL-producing uropathogenic *E. coli* is improved by combination with miconazole and polymyxin B nonapeptide, 65 (9 pages), BMC Microbiol. 14 (2014).

[27] H. Nurhasni, J. Cao, M. Choi, I. Kim, B.L. Lee, Y. Jung, J.W. Yoo, Nitric oxide-releasing poly(lactic-co-glycolic acid)-polyethylenimine nanoparticles for prolonged nitric oxide release, antibacterial efficacy, and in vivo wound healing activity, Int. J. Nanomed. 10 (2015) 3065–3080.

[28] Y. Sun, Y. Liu, W. Liu, C. Lu, L. Wang, Chitosan microparticles ionically cross-linked with poly(γ-glutamic acid) as antimicrobial peptides and nitric oxide delivery system, Biochem. Eng. J. 95 (2015) 78–85.

[29] E.M. Hetrick, J.H. Shin, N.A. Stasko, C.B. Johnson, D.A. Wespe, E. Holmuhamedov, M.H. Schoenfisch, Bactericidal efficacy of nitric oxide-releasing silica nanoparticles, ACS Nano 2 (2008) 235–246.

[30] G. Pezzotti, N. Oba, W. Zhu, E. Marin, A. Rondinella, F. Boschetto, B. McEntire, K. Yamamoto, B.S. Bal, Human osteoblasts grow transitional Si/N apatite in quickly osteointegrated Si_3N_4 cervical insert, Acta Biomater. 64 (2017) 411–420.

[31] G. Pezzotti, R.M. Bock, T. Adachi, A. Rondinella, F. Boschetto, W. Zhu, E. Marin, B. McEntire, B.S. Bal, O. Mazda, Silicon nitride surface chemistry: a potent regulator of mesenchymal progenitor cell activity in bone formation, Appl. Mater. Today 9 (2017) 82–95.

[32] B.R. Crane, J. Sudhamsu, B.A. Patel, Bacterial nitric oxide synthases, Annu. Rev. Biochem. 79 (2010) 445–470.

[33] I. Notingher, L.L. Hench, Raman microspectroscopy: a noninvasive tool for studies of individual living cells in vitro, Expet Rev. Med. Dev. 3 (2006) 215–234.

[34] L. Movileanu, J.M. Benevides, G.J. Thomas Jr., Temperature dependence of the Raman spectrum of DNA. Part I – Raman signatures of premelting and melting transitions of Poly(dA-dT).Poly(dA-dT), J. Raman Spectrosc. 30 (1999) 637–649.

[35] G.I. Dovbeshko, V.I. Chegel, N.Y. Gridina, O.P. Repnytska, Y.M. Shirshov, V.P. Tryndiak, I.M. Todor, G.I. Solyanik, Surface enhanced IR absorption of nucleic acids from tumor cells: FTIR reflectance study, Biopolymers 67 (2002) 470–486.

[36] A.C. Williams, H.G.M. Edwards, Fourier transform Raman spectroscopy of bacterial cell walls, J. Raman Spectrosc. 25 (1994) 673–677.

[37] A.C. Sekhar Talari, Z. Movasaghi, S. Rehman, I. ur Rehman, Raman spectroscopy of biological tissues, Appl. Spectrosc. Rev. 50 (2015) 46–111.

[38] C. Kajdas, General approach to mechanochemistry and its relation to tribochemistry, in: Tribol. Eng., INTEC, 2013, pp. 209–240.

[39] S. Mezzasalma, D. Baldovino, Characterization of silicon nitride surface in water and acid environment: a general approach to the colloidal suspensions, J. Colloid Interface Sci. 180 (1996) 413–420.

[40] J. Sonnefeld, Determination of surface charge density parameters of silicon nitride, Colloids Surf., A 108 (1996) 27–31.

[41] D.J. Arp, L.Y. Stein, Metabolism of inorganic N compounds by ammonia-oxidizing bacteria, Crit. Rev. Biochem. Mol. Biol. 38 (2003) 471–495.

[42] L.Y. Stein, Y.L. Yung, Production, isotopic composition, and atmospheric fate of biologically produced nitrous oxide, Annu. Rev. Earth Planet Sci. 31 (2003) 329–356.

[43] J.D. Caranto, K.M. Lancaster, Nitric oxide is an obligate bacterial nitrification intermediate produced by hydroxylamine oxidoreductase, PNAS 114 (2017) 8217–8222.

[44] G.L. Squadrito, W.A. Pryor, The formation of peroxynitrite in vivo from nitric oxide and superoxide, Chem. Biol. Interact. 96 (1995) 203–206.

[45] J. Depasse, J. Warlus, Relation between the toxicity of silica and its affinity for tetraalkylammonium groups – comparison between SiO_2 and TiO_2, J. Colloid Interface Sci. 56 (1976) 618–621.

[46] T. Jennison, M. McNally, H. Pandit, Review - prevention of infection in external fixation pin sites, Acta Mater. 10 (2014) 595–603.

[47] H. Dong, T. Mukinay, M. Li, R. Hood, S.L. Soo, S. Cockshott, R. Sammons, X. Li, Improving tribological and anti-bacterial properties of titanium external fixation pins through surface ceramic conversion, 5 (13 pages), J. Mater. Sci.: Mater. Med. 28 (2017).

[48] K. Page, M. Wilson, I.P. Parkin, Antimicrobial surfaces and their potential in reducing the role of the inanimate environment in the incidence of hospital-acquired infections, J. Mater. Chem. 19 (2009) 3818–3831.

[49] A. Fujishima, K. Hashimoto, T. Watanabe, *TiO_2 Photocatalysis*, Bkc Inc. Pub. Co., Tokyo, Japan, 2000.

[50] A. Mills, S. Lee, A web-based overview of semiconductor photochemistry-based current commercial applications, J. Photochem. Photobiol. Chem. 152 (2002) 233–247.

[51] J. Kiwi, S. Rtimi, R. Sanjines, C. Pulgarin, TiO_2 and TiO_2-doped films able to kill bacteria by contact: new evidence for the dynamics of bacterial inactivation in

the dark and under light irradiation, 785037 (17 pages), Int. J. Photoenergy 2014 (2014).
[52] T. Zubkoy, D. Stahl, T.L. Thompson, D. Panayotov, O. Diwald, J.T. Yates Jr., Ultraviolet light-induced hydrophilicity effect on TiO_2(110) (1×1). Dominant role of the photooxidation of adsorbed hydrocarbons causing wetting by water droplets, J. Phys. Chem. B 109 (2005) 15454–15462.
[53] R. Wang, K. Hashimoto, A. Fujishima, M. Chikuni, E. Kojima, A. Kitamura, M. Shimohigoshi, T. Watanabe, Light-induced amphiphilic surfaces, Nature 388 (1997) 431–432.
[54] F. Vatansever, W.C.M.A. de Melo, P. Avci, D. Vecchio, M. Sadasivam, A. Gupta, R. Chandran, M. Karimi, N.A. Parizotto, R. Yin, G.P. Tegos, M.R. Hamblin, Antimicrobial strategies centered around reactive oxygen species – bactericidal antibiotics, photodynamic therapy and beyond, FEMS Microbiol. Rev. 37 (2013) 955–989.
[55] A.W. Auner, J.C. Thomas, Double-stranded DNA damage assessed with Raman spectroscopy, 1000284 (7 pages), Biochem. Anal. Biochem. 5 (2016).
[56] F. D'amico, F. Cammisuli, R. Addobbati, C. Rizzardi, A. Gessini, C. Masciovecchio, B. Rossi, L. Pascolo, Oxidative damage in DNA bases revealed by UV resonant Raman spectroscopy, Analyst 140 (2015) 1477–1485.
[57] T. Theophanides, J. Anastassopoulou, The reaction of platinum antitumor compounds with DNA, in: M. Gielen (Ed.), Metal-based Antitumor Drugs, vol. 2, Freund Publishing House, London, UK, 1988, pp. 151–174.
[58] V. Krishnakumar, M. Arivazhagan, Vibrational and normal coordinate analysis of xanthine and hypoxanthine, Indian J. Pure Appl. Phys. 42 (2004) 411–418.
[59] N.H. Jang, The coordination chemistry of DNA nucleosides on gold nanoparticles as a probe by SERS, Bull. Kor. Chem. Soc. 23 (2002) 1790–1800.
[60] T. Ishida, Bacteriolyses of bacterial cell walls by Cu(II) and Zn(II) ions based on antibacterial results of dilution medium method and halo antibacterial test, J. Adv. Res. Biotech. 2 (2017) 1–12.
[61] R. Garcia-Contreras, L. Nunez-Lopez, R. Jasso-Chavez, B.W. Kwan, J.A. Belmont, A. Rangel-Vega, T. Maeda, T.K. Wood, Quorum sensing enhancement of the stress response promotes resistance to quorum quenching and prevents social cheating, ISME J. 9 (2015) 115–125.
[62] T. Kitao, Survey of methicillin-resistant coagulase-negative staphylococci isolated from the fingers of nursing students, J. Infect. Chemother. 9 (2003) 30–34.
[63] M. Otto, *Staphylococcus epidermidis* – the "accidental" pathogen, Nat. Rev. Microbiol. 7 (2009) 555–567.
[64] B.J. Privett, A.D. Broadnax, S.J. Bauman, D.A. Riccio, M.H. Schoenfisch, Examination of bacterial resistance to exogenous nitric oxide, Nitric Oxide 26 (2012) 169–173.
[65] A.B. Seabra, R. da Silva, M.G. de Oliveira, Polynitrosated polyesters: preparation, characterization, and potential use for topical nitric oxide release, Biomacromolecules 6 (2005) 2512–2520.
[66] A.B. Seabra, M.G. de Oliveira, Poly(vinyl alcohol) and poly(vinyl pyrrolidone) blended films for local nitric oxide release, Biomaterials 25 (2004) 3773–3782.
[67] H. Liang, P. Nacharaju, A. Friedman, J.M. Friedman, Nitric oxide generating/releasing materials, FSO54 (10 pages), Future Sci. OA 1 (2015).
[68] D.J. Smith, D. Chakravarthy, S. Pulfer, et al., Nitric oxide- 77 releasing polymers containing the [N(O)NO]- group, J. Med. Chem. 39 (1996) 1148–1156.
[69] D.D. Thomas, L.A. Ridnour, J.S. Isenberg, W. Flores-Santana, C.H. Switzer, S. Donzelli, P. Hussain, C. Vecoli, N. Paolocci, S. Ambs, C.A. Colton, C.C. Harris, D.D. Roberts, D.A. Wink, The chemical biology of nitric oxide: implications in cellular signaling, Free Radic. Biol. Med. 45 (2008) 18–31.
[70] N.A. Stasko, M.H. Schoenfisch, Dendrimers as a scaffold for nitric oxide release, J. Am. Chem. Soc. 128 (2006) 8265–8271.
[71] L.J. Taite, J.L. West, Poly(ethylene glycol)-lysine dendrimers for targeted delivery of nitric oxide, J. Biomater. Sci. Polym. Ed. 17 (2006) 1159–1172.
[72] R. Duncan, L. Izzo, Dendrimer biocompatibility and toxicity, Adv. Drug Deliv. Rev. 57 (2005) 2215–2237.
[73] D. Fischer, Y.X. Li, B. Ahlemeyer, J. Krieglstein, T. Kissel, In vitro cytotoxicity testing of polycations: influence of polymer structure on cell viability and hemolysis, Biomaterials 24 (2003) 1121–1131.
[74] R. Jevprasesphant, J. Penny, R. Jalal, D. Attwood, N.B. McKeown, A. D'Emanuele, The influence of surface modification on the cytotoxicity of PAMAM dendrimers, Int. J. Pharm. 252 (2003) 263–266.
[75] R.A.M. Serafim, M.C. Primi, G.H.G. Trossini, E.I. Ferreira, Nitric oxide: state of the art in drug design, Curr. Med. Chem. 19 (2012) 386–405.
[76] B. Sun, D.L. Slomberg, S.L. Chudasama, Y. Lu, M.H. Schoenfisch, Nitric oxide-releasing dendrimers as antibacterial agents, Biomacromolecules 13 (2012) 3343–3354.
[77] C. Napoli, G. Paolisso, A. Casamassimi, M. Al-Omran, M. Barbieri, L. Sommese, T. Infante, L.J. Ignarro, Effects of nitric oxide on cell proliferation, J. Am. College cardiol. 62 (2013) 89–95.
[78] G. Pezzotti, B.J. McEntire, R. Bock, W. Zhu, F. Boschetto, A. Rondinella, E. Marin, Y. Marunaka, T. Adachi, T. Yamamoto, N. Kanamura, B.S. Bal, In situ spectroscopic screening of osteosarcoma living cells on stoichiometry-modulated silicon nitride bioceramic surfaces, ACS Biomater. Sci. Eng. 2 (2016) 1121–1134.
[79] R.K. Poole, C. Kumar, I. Salmon, B. Chance, The 650 nm chromophore in *Escherichia coli* is an "oxy"- or oxygenated compound, not the oxidized form of cytochrome oxidase d: an hypothesis, J. General Microbiol. 129 (1983) 1335–1344.
[80] M.C. van Loosdrecht, J. Lyklema, W. Norde, G. Schraa, A.J. Zehnder, The role of bacterial cell wall hydrophobicity in adhesion, Appl. Environ. Microbiol. 53 (1987) 1893–1990.
[81] M. Ishikawa, K.L. de Mesy Bentley, B.J. McEntire, B.S. Bal, E.M. Schwarz, C. Xie, Surface topography of silicon nitride affects antimicrobial and osseointegrative properties of tibial implants in a murine model, J. Biomed. Mater. Res. Part A 105 (2017) 3413–3421.